

Molecular BioSystems

Accepted Manuscript



This is an *Accepted Manuscript*, which has been through the Royal Society of Chemistry peer review process and has been accepted for publication.

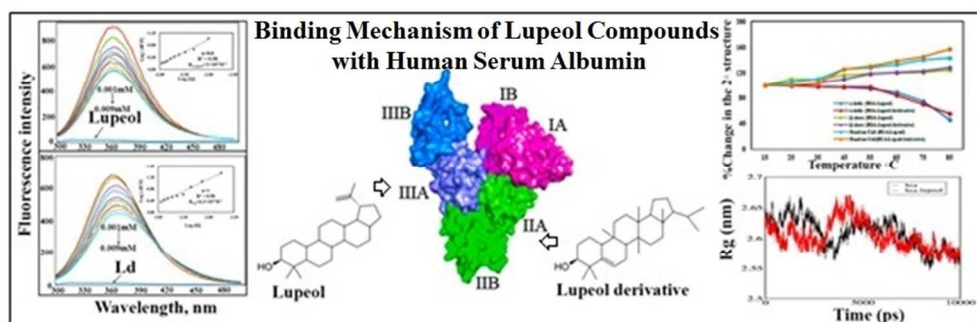
Accepted Manuscripts are published online shortly after acceptance, before technical editing, formatting and proof reading. Using this free service, authors can make their results available to the community, in citable form, before we publish the edited article. We will replace this *Accepted Manuscript* with the edited and formatted *Advance Article* as soon as it is available.

You can find more information about *Accepted Manuscripts* in the [Information for Authors](#).

Please note that technical editing may introduce minor changes to the text and/or graphics, which may alter content. The journal's standard [Terms & Conditions](#) and the [Ethical guidelines](#) still apply. In no event shall the Royal Society of Chemistry be held responsible for any errors or omissions in this *Accepted Manuscript* or any consequences arising from the use of any information it contains.



www.rsc.org/molecularbiosystems



Binding of Lupeol Compounds with Plasma Proteins
279x95mm (96 x 96 DPI)

Comparative Binding Mechanism of Lupeol Compounds with Plasma Proteins and its Pharmacological Importance

Monika Kallubai^a, Aparna Rachamalla^b, Daniel Pushparaju Yeggoni^a, Rajagopal Subramanyam^{a*}

^a *Department of Plant Sciences, School of Life Sciences, University of Hyderabad, Hyderabad 500046, India*

^b *National Institute of Animal Biotechnology, Axis Clinicals Building, Miyapur, Hyderabad, 500049, India*

*Corresponding author
Rajagopal Subramanyam
Department of Plant Sciences
School of Life Sciences
University of Hyderabad 500 046 India
Tel: +91-40-23134572
Fax: +91-40-23010120
Email: srgsl@uohyd.ernet.in

Abstract

Lupeol a triterpene, possesses beneficial effects like anti-inflammatory and anti-cancer properties. Binding of lupeol and its derivative to plasma proteins such as human serum albumin (HSA) and α -1-acid glycoprotein (AGP) is a major determinant in the disposition of drugs. Cytotoxic studies with mouse macrophages (RAW 246.7) and HeLa cell lines revealed anti-inflammatory and anti-cancer properties for both lupeol and lupeol derivative. Both molecules reduced the expression of pro-inflammatory cytokines in LPS induced macrophages. Further, apoptosis was observed from HeLa cell lines when the molecules incubated for 24 h. The fluorescence quenching of HSA was observed upon titration with different concentrations of lupeol and lupeol derivative; their binding constants were found to be $3 \pm 0.01 \times 10^4 \text{ M}^{-1}$ and $6.2 \pm 0.02 \times 10^4 \text{ M}^{-1}$, with binding free energies of $-6.59 \text{ kcal M}^{-1}$ and -7.2 kcal M^{-1} . With AGP, however, the lupeol and lupeol derivative showed binding constants of $0.9 \pm 0.02 \times 10^3 \text{ M}^{-1}$ and $2.7 \pm 0.01 \times 10^3 \text{ M}^{-1}$, with free energies of -4.6 kcal M^{-1} and -5.1 kcal M^{-1} respectively. Molecular displacement studies based on competition with site I-binding phenyl butazone (which binds site I of HSA) and ibuprofen (which binds site II) suggest that lupeol binds in site II, and lupeol derivative in site I. Molecular docking studies also confirmed that lupeol binds to the IIIA and lupeol derivative to the IIA domain of HSA. Secondary structure changes were observed upon formation of HSA-lupeol/derivative complexes by circular dichroism spectroscopy. Molecular dynamics simulations support greater stability of HSA-lupeol and HSA-lupeol derivative complexes compared to HSA alone.

Keywords: Human serum albumin, α -1-acid glycoprotein, Cytotoxic, Phytocompounds, Molecular docking, Molecular dynamics simulations

Introduction

Lupeol, a monohydroxylated pentacyclic triterpenoid found in fruits, vegetables and medicinal plants possesses strong clinical properties. Lupeol isolated from the leaves of *Aegle marmelos* appeared to be a good drug for antidiabetic, antihyperglycemic¹ and even hypercholesterolemia². Lupeol is a diet-derived agent (acceptable to human), nontoxic and bioavailable, and a dose tailored treatment was successful in the treatment of prostate cancer³. It also reduced the growth of granulomatous growth of the synovium and the severity of cartilage and subchronal bone erosion associated with the adjuvant arthritis⁴. Pentacyclic triterpenes have been widely reported to exhibit anti-inflammatory activities⁵. Recently, it has been proved that changes in the pentacyclic ring, and the strength of hydrogen bonding capability or acidity at C-19, C-20 and C-28 positions confirmed differences in biological activities of lupeol⁶. Thus, lupeol had a wide range of pharmacological action; distribution of these molecules and their activity are controlled by their strong binding to proteins in the systemic circulation after oral absorption. Thus, the interactions of small molecules with proteins which results in the formation of complexes modify protein properties and structure have been a target of research.

Human serum albumin (HSA) and α -1 acid glycoprotein (AGP) are the predominant proteins in human blood plasma. HSA has 585 amino acid residues and exists as a monomer of molecular mass 66 kDa with 3 domains: domain I (Residues 1–195), domain II (196–383) and domain III (384–585). Each domain can be subdivided into subdomains A and B, possessing common structural motifs. The protein is stabilized by 17 disulfide bridges, resulting in a heart-shaped tertiary structure^{7,8}. HSA is the most abundant plasma protein and is known for its capability to serve as carrier for a number of ligands like fatty acids, hormones and many drugs^{9,10}. HSA binding often results in an increased solubility in plasma, decreased toxicity, protection

against oxidation, and prolonged *in vivo* half-life of the bound ligands¹¹. HSA has multiple ligand-binding sites localized in these subdomains^{12, 13}. Two primary drug-binding sites have been characterized: subdomains IIA and IIIA, also known as Sudlow's site I and Sudlow's site II. These two sites received attention due to their high drug-binding affinity; site I is dominated by strong hydrophobic interactions with neutral, bulky, heterocyclic compounds, while site II binds mainly by dipole-dipole, van der Waals, and/or hydrogen-bonding interactions with aromatic carboxylic acids¹⁴⁻¹⁶. Phytocompounds like β -sitosterol, coumaryltyramine, asiatic acid, coumarin derivatives and methimazole show binding to Sudlow's site I (IIA), which is the major drug binding site on HSA¹⁷⁻²¹, whereas other phytocompounds like trimethoxyflavone and ginsenoside Rg3^{22, 23} bind to Sudlow's site II (IIIA). Interestingly, synthetic 7-hydrocoumarin derivatives also bind to the same subdomains (7HC-1 to IIIA, 7HC-2 to IIIB and 7HC-3 to IIIB)²⁴. Recent reports show that the IB site is also a good candidate for the binding of other drug molecules including fatty acids and endogenous substances such as the hormones thyroxine, bilirubin and hemin molecules^{13, 25, 26}. Our group has reported various coumarin derivatives and trans-feruloyl maslinic acid interacting with HSA via domain I^{20, 27}. Hence, HSA is a promiscuous ligand binder, with a surprising capacity to bind a large variety of biologically active molecules.

Another important plasma protein, AGP (also known as orosomucoid), is a 44 kDa single polypeptide encompassing 183 amino acid residues. It belongs to the lipocalin family of proteins, a heterogeneous group of extracellular proteins that bind a variety of small hydrophobic ligands^{28, 29}. AGP is synthesized in the liver and secreted into the blood stream at concentrations of 0.6-1.2 mg/ml, which is approximately 1-3% of total protein; HSA comprises 60% of the plasma proteins^{30, 31}. AGP is greatly elevated under inflammatory or other pathological conditions, and

is able to bind basic drugs³². Still, the detailed characteristics of binding sites on HSA and AGP are not yet clear.

Since lupeol compounds possess strong anti-oxidant, anti-inflammatory, anti-arthritic, anti-mutagenic, anti-tumor and anti-malarial properties, we confirmed the anti-inflammatory and anti-cancer properties of lupeol and its derivative through cytotoxic studies. Further, the interactions of lupeol and its derivative with HSA and AGP has been studied using spectroscopic methods. Lupeol derivative is structurally similar to lupeol, except for a double bond between the carbon atoms at positions C3 and C7. To support our experimental studies and provide more structural details, molecular docking and dynamics simulations were performed. Our work should be helpful to understand the pharmacokinetic and pharmacodynamics aspects of lupeol treatment, as well the ability of derivatives of natural compounds to improve their immunomodulatory activities.

Materials and Methods

Preparation of stock solutions

Pure fat-free HSA (purchased from Sigma Aldrich) was prepared to 1.5 mM concentration dissolved in 0.1 M phosphate buffer at pH 7.4. Lupeol and lupeol derivative (phytocompounds) was purchased from Natural Remedies Pvt., Ltd, Bengaluru India, with a purity of 95%. Its stock solution ($1.0 \times 10^3 \text{ M}^{-1}$) was prepared in 20:80 ethanol:water mixture. The molecular weight of Lupeol and lupeol derivative is same 426.7 Da, while structurally lupeol derivative had a difference in the double bond arrangement between C5 and C6 atoms. The optimum pH for HSA was set to be 7.4 as it has the maximum absorption at this pH^{27,33}. Thus for all the experiments, we have used 0.1 M phosphate buffer at pH 7.4 as a physiological buffer. All other chemicals are of analytical grade purchased from Sigma Aldrich.

Cell response assay (MTT assay)

To understand anti-inflammatory and anti-cancer property, a cell response assay was carried out using 3-(4,5-dimethylthiazol-2-yl)-2,5-diphenyltetrazolium bromide (MTT) staining method³⁴. LPS induced mouse macrophage cells (RAW 264.7) and human cervical cancer cells (HeLa) were sub-cultured and seeded in 96 well plates at a density of 5×10^3 cells. Lupeol and its derivative were added to the above plates in a dose dependent manner (from 10 μ M to 100 μ M) and the effect was tested for 48 hrs, a control was maintained without the addition of lupeol and its derivative. After 48 hours 20 μ L (5mg/ml in PBS) of MTT was added and cells were incubated further for 4 hours. To dissolve the MTT crystals 100 μ L of DMSO was added to each well and mixed with repeated pipetting. The Cell response was measured at 570 nm optical absorbance on a micro plate reader (μ Quant Bio-tek Instrument, Inc.). The same experiments were performed three times, in triplicates each time; changes in the cell responses were noted using control as reference. The mean \pm SE was calculated and reported in terms of the cell response (%) vs concentration (μ M).

Determination of cytokines production

We investigated the biological effects of lupeol and lupeol derivative on inflammatory cytokines IL-1 β and IL-6 using mouse ELISA kit (R&D systems, 210331). Mouse macrophages (RAW264.7) were pretreated with lupeol and lupeol derivative for 1h and then LPS was added at 1 μ g/mL concentration and further incubated for 5h. Supernatant was collected and used for the estimation of cytokines. The inhibitory effect of lupeol and lupeol derivative was determined by an ELISA reader at 570 nm absorbance.

Apoptosis Evaluation for anticancer activity

Cell death was measured by using Annexin V-FITC detection Kit (Sigma cat no: APOAF). HeLa cells were treated with half the concentration of IC50 values of lupeol and its derivative for 24 h, later cells were washed twice with phosphate buffer saline, then resuspended in binding buffer and stained with 5 μ l of Annexin V-FITC. It conjugate with fluorescent isothiocyanate (FITC) to label phosphatidylserine sites on the membrane surface and 10 μ l of Propidium Iodide for 10min to label the cellular DNA in necrotic cells, where the cell membrane is almost disrupted³⁵.

Room temperature fluorescence spectra measurements

Protein-drug interactions can affect the molecular biological activity and function of proteins³⁶. Fluorescence emission measurement is one method to help understand protein-drug binding. A Perkin Elmer LS-55 fluorimeter was used to measure fluorescence spectra with a 1.0 cm quartz cuvette. For both HSA and AGP, the excitation wavelength was 285 nm and emission spectra were recorded at 25° C in the range of 300-500 nm; bandwidths for both excitation and emission were 10 nm. A fixed concentration (0.001 mM) of HSA and AGP with different concentration of lupeol from 0.001 to 0.009 mM in 0.1 M phosphate buffer solution was used at physiological pH of 7.4. The incubation of each concentration of lupeol with HSA and AGP was 5 minutes. The experiments were repeated twice for both lupeol and lupeol derivative, and each time approximate spectrum values were obtained. Binding constants were calculated using fluorescence intensity at the emission maximum (340 nm for AGP and 360 nm for HSA).

Molecular displacement experiment

Many drugs can bind to the same HSA drug binding sites or to different functionally linked clefts either competitively or synergistically. Identifying the drug binding site is important to

understand the efficacy of drug delivery. Site-competitive replacement experiments were carried out to understand the binding site of drug molecules to HSA using site specific markers (phenyl butazone and ibuprofen for site I and site II, respectively). HSA and the binding site probe were maintained at a concentration of 1 μM , whereas lupeol and lupeol derivative were titrated with an increase in concentration from 0.001 to 0.009 mM. The excitation wavelength is 285 nm for site specific markers phenyl butazone, ibuprofen and HSA as well, and the data were measured using the modified Stern-Volmer equation^{24, 37}.

Circular dichroism measurements

HSA and HSA-lupeol complex secondary structures were measured by using Jasco J-810 spectropolarimeter (a Quartz cuvette with 0.02 mm path length under nitrogen atmosphere), and spectra were recorded in the region of 190-260 nm, with a scan speed of 100 nm min⁻¹. The concentration of HSA was fixed at 0.001 mM, while the lupeol and its derivative were added in an increasing concentration of 0.001, 0.002 and 0.003 mM. Jasco J-715 peltier was used for measuring temperature dependent circular dichroism spectra for HSA-lupeol and its derivative complexes with increasing temperature of 25-85⁰C. The web-based software CDNN 2.1 was used to predict the percentages of secondary structure of α -helix, β -sheet and random coil of pure HSA as well as the HSA-lupeol and HSA-lupeol derivative complexes.

Molecular modeling and docking

The crystal structure of HSA (PDB ID: 1AO6) was obtained from the Protein Data Bank. 3-dimensional structure of lupeol and its derivative was built, and its geometry was optimized through Discovery Studio 3.5 in InsightII/Builder. Structures were optimized and used as input for AutoDock Tools. To find the binding site and types of interactions involved in the formation of HSA-lupeol and HSA-lupeol derivative complexes, docking was performed using the

Lamarckian genetic algorithm implemented in AutoDock 4.2. We found this to be the best-performing docking method in terms of its ability to find the lowest energy and its structure prediction accuracy; it also incorporates ligand flexibility^{38, 39}. AutoDock 4.2 takes water as solvent by default, and polar hydrogens were added using the MGL tools interface. Blind docking was carried out using the AutoGrid utility; the docking area was defined by a box with grid spacing of 0.586 Å and the dimension of 126×126×126 Å with points along the x, y and z axes. The docking parameters are: number of individuals in the population (set to 150); maximum number of energy evaluations (set to 2,500,000), and maximum number of generations (set to 2700), and number of genetic algorithm runs (set to 30). For each docking simulation, 30 different conformers were generated, and the obtained conformations were analyzed for the lowest free energy conformer, which is considered to be close to the experimentally determined free energy values reported^{24, 40}. LIGPLOT was used for plotting protein–ligand interactions, and also to analyze hydrophobic and hydrogen bond interactions between HSA-lupeol and HSA-lupeol derivative⁴¹. The same procedure was repeated for all the three structures to understand the same binding modes and found no difference as the domains are conserved in all the structures present in PDB data bank. Also 42 structures of human serum albumin present in PDB were analyzed through dynamics simulations and concluded that binding of small molecules does not induce significant structural changes⁴². Thus the docking complexes with crystal structure 1AO6 are selected for further studies.

Molecular dynamics simulations (MD)

The initial configurations used for MD simulations of the HSA-lupeol and lupeol derivative complexes were the lowest-energy docked structures, with energies very close to the experimental binding energies and binding constants. The Gromacs v4.6.3 package with force

field GROMOS96 43a1⁴³, was used for unliganded HSA, HSA-lupeol and HSA-lupeol derivative complexes. Further, PRODRG2.5 server (beta) was used to build the topology parameter of lupeol and lupeol derivative⁴⁴. Missing atoms were added to the initial coordinates of the complexes, and the topology file was generated. During simulations, each complex was placed in the center of a box with appropriate dimensions of 80×80×80 Å and water molecules were added to fill the box using SPC⁴⁵, yielding a total system size of 5843 atoms. All protein side chains were assumed to be in their default ionization states based on pKa calculations⁴⁶. Sodium counter ions were added to each simulation box to maintain electro-neutrality and to release conflicting contacts. Energy minimization was performed using the steepest descent method for 1000 steps and conjugated gradient method for the subsequent 1000 steps.

Simulations were performed in the NPT ensemble, at a temperature of 300 K maintained using a Berendsen thermostat⁴⁷ with a coupling constant of 1.0 ps. Protein and water/ions were coupled independently. Pressure coupling used the Berendsen barostat with a coupling constant of 1.0 ps. Long-range electrostatic interactions were calculated using the particle mesh Ewald method⁴⁸ with a 10 Å cut-off. LINCS algorithm⁴⁹, was used to restrain bond lengths. Each system was energy minimized followed by a short 200 ps simulation during which the protein, and if present ligand, non-hydrogen atoms were harmonically restrained with a force constant of 1000 kJ/mol/Å². All restraints were then removed and each simulation was run for 10 ns; simulation and analysis were performed on Linux cluster with 36 nodes (dual Xeon processor) at the Bioinformatics facility of the University of Hyderabad.

Results and discussion

Cell viability assay

Evidence obtained from experiments on human melanoma cells indicate that lupeol has anti-cancer properties⁵⁰. Vasconcelos et al.⁵¹ confirmed that lupeol has potent anti-inflammatory activity by a significant reduction in eosinophils infiltration and in Th2-associated cytokines (IL-4, IL-5, IL-13) levels that trigger the immune responses in asthma. To reconfirm the importance of lupeol molecules, we performed a cell viability assay by the MTT staining method, to test anti-inflammatory property of lupeol and lupeol derivative (phytocompounds) on the mouse macrophage (RAW 264.7) cell line. Our results indicated that the lupeol inhibits inflammation with increasing concentrations of 20, 40, 60, 80 and 100 μM for 48 h in a final volume of 100 μl . In a negative control, cells were grown in media without lupeol and its derivative. The results showed anti-inflammatory response with an IC_{50} value of 80 μM for lupeol, whereas lupeol derivative had an IC_{50} value of 63 μM (Fig. 1A and 1B). Thus, lupeol derivative showed stronger inhibition of the growth of inflamed macrophages compared with lupeol. We have also tested anticancer property on human cervical cancer cell lines (HeLa), and examined the effects of lupeol and lupeol derivative on the viability of these cells by using the above method. A decrease in cell viability with both the molecules in a dose-dependent manner was observed, and the effect of these molecules represented with an IC_{50} values for lupeol and lupeol derivative was 30 μM and 24 μM , respectively (Fig. 1C and 1D). We also, carried out these compounds on HepG2 cells lines (hepatic carcinoma) but observed no effect.

Cytokines studies of lupeol compounds

We further evaluated the inhibitory effect of lupeol and lupeol derivative on the expression of inflammatory cytokines IL-1 β and IL-6 by ELISA. As shown in the (Fig. S1), both IL-1 β and IL-6 cytokines expression was down regulated by lupeol and lupeol derivative compared to the LPS induced cells. However, the lupeol derivative is showing stronger inhibition of cytokines in a

dose dependent manner compared to lupeol. With same cytokines (IL-1 β and IL-6) we have tested for HeLa cell lines to understand the anti-cancer role; however, we did not see any significant effect. This could be explained that for cancer, there are several other cytokines are involved which may be studied in future.

Apoptotic studies from HeLa cell lines

Anticancer drugs can potentially kill cells in different ways by interfering with cellular process, essential for cell viability and triggering an endogenous physiological cell death mechanism. Further, we tested lupeol and lupeol derivative for induction of apoptosis from HeLa cell lines, which is a morphological and biochemical distinct form of programmed cell death in many cells. The normal cells contain phosphatidylserine residues in the inner membrane of cytoplasm and during apoptosis of these residues are translocated and are exposed, an early event in apoptosis. Annexin V is known to be phosphatidylserine-binding protein available conjugated with FITC to label phosphatidylserine sites on the membrane surface. Propidium Iodide binds to cellular DNA in cells, where the cell membrane is totally damaged. The number of cell replications was assessed with the aid of fluorescent dye, which covalently binds to cytoplasmic components of cell resulting green fluorescence, and the resolution can be allowed upto eight cycles of cell division, which can be detected by flow cytometry. In our study, half the concentration of IC50 values from cell viability assay was treated with lupeol and its derivative, 15 and 12 μ M respectively for 24h to measure the cell death by using apoptotic detection kit as described in methods. The results are shown as dot-plot representation (FITC-A on x-axis and PE-A on y-axis) in quadrants and histogram (Fig. 2). The results showed that percent apoptotic cells are 0.8 with lupeol, while 2.6% for lupeol derivative, which is more than two fold cell death than lupeol. The percentages of different cells in quadrants are given in Table S1. Our results suggest that

lupeol derivative could be effective than lupeol in its anticancer activity. Further insights into the molecular mechanisms that mediate the antitumor activities were needed to promote their development as chemo preventive agents and cancer therapeutics in the ongoing battle against cancer.

Analysis of fluorescence emission data

Anti-inflammatory drugs are known to bind to HSA with high affinity^{14, 52}, so it is necessary to understand the protein-drug interactions, as the lupeol and lupeol derivative are known to be highly anti-inflammatory and anti-cancer drugs. Fluorescence spectroscopic methods are the primary research tools in biochemistry and biophysics to measure protein-drug interactions. The fluorescence spectra of HSA in the absence and presence of lupeol and lupeol derivative were measured; HSA showed a strong fluorescence emission at 360 nm ($\lambda_{\text{ex}} = 285$ nm) while both drugs were almost non-fluorescent (Fig. 3A and 3B). Increasing lupeol concentrations resulted in a lowering of HSA fluorescence intensity, with slight decrease in maximum emission, which clearly indicated that the binding of the lupeol to HSA changed the microenvironment around the tryptophan residue. Previously it has been stated that, the fluorescence is due to amino acid residues, tryptophan, tyrosine, and phenylalanine, out of which tryptophan plays a major role in the intrinsic fluorescence of HSA, because of low quantum yield of phenylalanine. The fluorescence of tyrosine is almost quenched if it is ionized or near an amino group, a carboxyl group, or a tryptophan⁵³.

A nonlinear relationship between the observed fluorescence intensity and concentrations (Q) of lupeol and lupeol derivative was resulted with an increase in the concentrations of lupeol and its derivative with both HSA and AGP, which increased the absorbance of excitation, and

emission radiation-inducing the inner filter effect that may decrease the intensity of fluorescence.

The inner filter effect can be corrected by using following equation

$$F_{\text{cor}} = F_{\text{obs}} 10^{(A_{\text{exc}} + A_{\text{emi}})/2} \quad [1]$$

Where, F_{cor} and F_{obs} are the fluorescence intensity corrected and observed, A_{exc} and A_{emi} represent the absorbance at the fluorescence excitation (285 nm) and emission wavelengths 360 nm. In order to understand the fluorescence quenching mechanism (static or dynamic) of HSA-lupeol, and HSA-lupeol derivative complexes, the quenching data were analyzed using the Stern-Volmer equation,

$$F_0/F = 1 + k_q t_0 [Q] = 1 + K_D [Q] \quad [2]$$

where F and F_0 are the fluorescence intensities in the presence and absence of quencher, $[Q]$ is the quencher concentration, and K_D is the Stern-Volmer quenching constant (K_q), which can be written as $K_D = k_q t_0$; where k_q is the bimolecular quenching rate constant and t_0 is the lifetime of the fluorophore in the absence of quencher is 5.6 ns⁵⁴. From the above equation the quenching constant was calculated to be $5.08 \times 10^{13} \text{ M}^{-1} \text{ s}^{-1}$ for lupeol and $5.5 \times 10^{13} \text{ M}^{-1} \text{ s}^{-1}$ for lupeol derivative. Thus the quenching mechanism is static, as these values are much greater than the maximum collisional quenching constant $2.0 \times 10^{10} \text{ M}^{-1} \text{ s}^{-1}$ ⁵⁵ (Fig.S2). Since lupeol and lupeol derivative induced fluorescence quenching of HSA as a static process, the binding constant (K) and the number of bound complexes to HSA (n) were determined by plotting the fluorescence data using modified Stern-Volmer equation⁵⁶.

$$\log (F_0 - F)/F = \log K_s + n \log [Q] \quad [3]$$

Where Q , n and K_s denoted as quencher concentration, number of binding sites and binding constant, respectively. Our results showed linear graph plotted with $\log [(F_0 - F)/F]$ versus $\log [Q]$, which indicates HSA-lupeol and HSA-lupeol derivative binding are one-to-one interaction with

HSA, supporting static quenching. From the intercept, binding constants of lupeol and lupeol derivative with HSA were calculated to be $K_{Lup} = 3 \pm 0.01 \times 10^4 \text{ M}^{-1}$ and $K_{Ld} = 6.2 \pm 0.02 \times 10^4 \text{ M}^{-1}$ for lupeol and lupeol derivative (Fig. 3A and 3B). Our results are in agreement to the previous studies with flavonoids-displaying binding constant in the range of $1-5 \times 10^4 \text{ M}^{-1}$ ⁵⁷. These binding constants K are further used to calculate the standard free energy with an equation as follows:

$$\Delta G^0 = -RT \ln K \quad [4]$$

where ΔG^0 is free energy change, K is binding constant at temperature 298 K, and R is the gas constant. The calculated free energy for lupeol and lupeol derivative are $-6.59 \text{ kcal M}^{-1}$ and -7.2 kcal M^{-1} , respectively. These values compare reasonably with computationally calculated free energies ($-6.45 \text{ kcal M}^{-1}$ and $-6.89 \text{ kcal M}^{-1}$). This indicates that the lupeol molecules bind to the protein mainly by hydrophobic interactions. Similar results were observed from our laboratory with different molecules like β -sitosterol, coumaryltyramine, asiatic acid, coumarin derivatives, trimethoxy flavone, 7-hydroxycoumarin derivatives and chitosan oligomers, which all bind to HSA^{17-20, 22, 24, 58}.

Since AGP is an acute phase protein and most of the drugs also bind to this protein during pathological conditions, we have checked the binding of lupeol to AGP. When lupeol molecules were titrated with AGP the fluorescence maximum (340 nm) was quenched upon increasing concentration of lupeol (Fig. 4A and 4B). This indicates that both lupeol and lupeol derivative also bind to AGP, but with lower binding constants than with HSA, i.e. $0.9 \pm 0.02 \times 10^3 \text{ M}^{-1}$ and $2.7 \pm 0.01 \times 10^3 \text{ M}^{-1}$ for lupeol and lupeol derivative. However, these binding constants are in the range of FDA (Food and Drug Administration) i.e. $10^3 - 10^5 \text{ M}^{-1}$ ¹⁵. The free energies obtained

were found to be -4.6 kcal M^{-1} and -5.1 kcal M^{-1} , respectively. The above results indicate that these phytochemicals bind efficiently to the plasma proteins HSA and AGP.

Molecular displacement studies for site-specific binding

Generally there are several site specific fluorescence probes (warfarin, ibuprofen, diazepam, phenyl butazone, ketoprofen) to find out the exact binding pocket of HSA⁵⁹. Warfarin, an anti-coagulant drug, and ibuprofen, a non-steroidal anti-inflammatory agent, are considered as stereotypical ligands for Sudlow's site I and Sudlow's site II, respectively. Hence, in order to identify the precise binding site of HSA with lupeol molecules, phenyl butazone and ibuprofen were used as site marker fluorescence probes for monitoring site I and II. In site-competitive replacement experiments, the concentration of HSA and site specific marker are kept at equal concentration (0.001 mM) and titrated with lupeol and lupeol derivative at increasing concentrations. The fluorescence intensities are measured and analyzed. The titration of the different concentration of lupeol to HSA-ibuprofen decreased the fluorescence emission quenching; binding constant values for lupeol-HSA were found to be $1.8 \pm 0.01 \times 10^4 \text{ M}^{-1}$ (Fig. 5A), while it did not show any competition with phenyl butazone. Lupeol derivative showed replacement of phenyl butazone (Fig. 5B) with a binding constant of $3.3 \pm 0.02 \times 10^4 \text{ M}^{-1}$; these values are close to the above experimental values ($3 \pm 0.01 \times 10^4 \text{ M}^{-1}$ and $6.2 \pm 0.02 \times 10^4 \text{ M}^{-1}$) obtained from fluorescence emission. These results revealed that there is a competition between lupeol and ibuprofen between lupeol derivative and phenyl butazone, suggesting that subdomain IIIA (Sudlow's site I) is the site for lupeol binding and subdomain IIA (Sudlow's site II) for lupeol derivative. Our experimental data is consistent with the docking studies that show lupeol and lupeol derivative binding to the IIIA and IIA domains.

Secondary structure analysis by using circular dichroism data

The phenomenon of circular dichroism (CD) is a sensitive technique to identify the secondary structure of polypeptides and proteins. CD spectroscopy is a form of light absorption spectroscopy that measures the difference in absorbance of right- and left-circularly polarized light by a substance. It has been shown that CD spectra between 260 and approximately 180 nm can be analyzed for the different secondary structural types: α -helix, parallel and antiparallel β -sheets, β -turns, and others. The CD spectra of HSA with various concentrations of lupeol and lupeol derivative in PBS (pH = 7.4) were taken at room temperature (Fig. 6). It can be seen from the figure that HSA exhibits two negative bands at 208 and 222 nm respectively, which are characteristic of the α -helices, and both contributed to $n-\pi^*$ transfer for the peptide bond of the α -helical structure⁶⁰. The secondary structure protein conformation found to be 58% α -helix, 20% β -sheet (including parallel and anti-parallel) and 22% random coil for HSA and which are closer to the previous reports^{18, 22, 24}. It also indicated that conformational changes occur in HSA upon complexation with lupeol and lupeol derivative. The secondary structure elements from HSA and HSA-lupeol, HSA-lupeol derivative complex formation, were calculated by CDNN software. Fig. 6A and 6B shows the complexation of HSA upon with titration of lupeol and lupeol derivative (0.003mM), after complexation there is a decrease in α -helical content from 58 to 50.5 ± 1.8 and $44.3\% \pm 1.0$, while β -sheets increased from 20 to 24 ± 0.1 and $26.6\% \pm 2.1$ and random coils from 22 to 24 ± 0.1 and $26.6\% \pm 0.2$, respectively. The percentages of the values obtained for α -helix, β -sheet, random coils of lupeol and lupeol derivative are calculated and are shown in Fig. 6C, and the data points are given in Table S2. The order of structural changes in α -helical is in the ascending order, is as follows lupeol derivative > lupeol where lupeol derivative > lupeol as the β -sheets and random coils lupeol derivative > lupeol. The conformational changes upon complexation of HSA+lupeol derivative may be due to minor unfolding of the protein,

which is very common in ligand binding. Thus, the difference in α -helical content might be due to structural rearrangements or changes in the microenvironment around tryptophan upon protein-ligand complex formation. To further investigate these changes, MD simulations were performed to visualize the structural changes in the protein. Our results corroborated with our previous reports with similar conformational changes, while binding of coumarin derivatives and 7-hydroxycoumarin derivatives and chitosan oligomers with HSA^{20, 24, 58}.

Temperature-dependent CD was carried out for HSA and HSA with 0.003 mM lupeol and lupeol derivative, from 25–85 °C to resolve the stability of these complexes. The secondary structural conformation of the protein was not significantly changed up to 65 °C in HSA-lupeol, and HSA-lupeol derivative complexes. Above 65 °C, the α -helical content decreased dramatically, while the random coil content increased in both complexes (Fig. S3). Earlier report showed that the T_m of the HSA alone was around 65 °C, which shows that the unfolding of protein occurs only after this point⁶¹. This data reveals that HSA-lupeol derivative complexes are very stable and thus, it can be a good candidate to deliver the drugs very efficiently even in adverse conditions.

Molecular docking studies

The information of protein-ligand binding sites is very important not only for revealing true binding mechanisms but also for rational drug design. To facilitate this, computational methods such as docking and MD simulation are among the best approaches for the estimation of molecular insights and the validation of experimental results. Molecular docking was carried out to bind lupeol and lupeol derivative to HSA structure. The most favorable conformation (the one with the lowest docked energy) found in the 30 independent docking runs, was taken on the basis of free energy assessment estimated by intermolecular energy (including van der Waals energy,

hydrogen bonding energy and electrostatic energy), internal energy, and torsional free energy. Also, the lowest binding energy conformer obtained from docking results ($-6.45 \text{ kcal M}^{-1}$ and $-6.89 \text{ kcal M}^{-1}$, lupeol and lupeol derivative) was closely matching to the experimentally determined values ($-6.59 \text{ kcal M}^{-1}$ and -7.2 kcal M^{-1} lupeol and lupeol derivative). Among the best conformers the lowest binding energy conformer is assessed for the binding site in receptor (HSA) using LIGPLOT, as the HSA contains two drug-binding sites, namely site I and site II located in hydrophobic cavities in subdomains IIA and IIIA, respectively^{8, 14}. In the best conformer, lupeol is surrounded by residues Pro416, Gln417, Tyr497, Val469, Ser470, Asp494, Thr496 and Val498, and Asp471 is stabilized by one hydrogen bond. The residues listed are part of domain III (384-585) i.e. site II^{8, 62}. Further, lupeol derivative showed binding to site I, domain II (196-383), forming hydrogen bonds with Ala300 and Pro299, and surrounded by Met298, Asp301, Leu302, Pro303, Ser304, Leu305, Tyr334, Arg337, Tyr341, and His338 (Fig. 7C and 7F). When predicting the posing of a ligand into a protein, docking can provide a good starting point to understand the preferred orientation of sterically acceptable ligands with protein. Both lupeol and lupeol derivative are structurally similar except a difference in the double bond arrangement, but the binding poses are different and are shown in Fig. 7B and 7E, which explains that lupeol structure was stabilized by chair conformation and the unsaturated double bond present outside the ring does not affect the hydrogen bond formation, whereas unsaturated double bond in the ring of lupeol derivative causes restricted rotation of molecule, and double bond adjacent to OH group decreases the electron withdrawing capability of oxygen resulting in formation of hydrogen bond with two basic amino acids. Essentially, because of this reason the orientation of lupeol derivative changed to bind in site I instead of site II.

Also we have performed the docking with two more structures i.e. 2BXC and 1BM0 and analyzed the binding modes and binding energies. Free energies obtained from docking studies with PDB ID: 2BXC showed as $-6.37 \text{ Kcal M}^{-1}$ and -7.1 Kcal M^{-1} for lupeol and lupeol derivative. Also, from PDB ID: 1BM0 showed as $-6.88 \text{ kcal M}^{-1}$ and $-7.03 \text{ kcal M}^{-1}$ for lupeol and lupeol derivative, respectively when they bound to site II and site I (data not shown). Thus, same binding modes are obtained even if we tried with other PDB's of HSA since they have similar binding pockets for all the crystal structures. Further, molecular displacement studies confirm that lupeol binds in site II and lupeol derivative in site I (Fig. 5), in agreement with the computationally determined docking studies. Thus the result of molecular modeling study is in good accordance with the experimental study.

Molecular dynamics simulations studies

Molecular dynamics simulations (MD) have become a promising tool to generate multiple conformations for the investigation of macromolecules, as they can provide insights of the molecular properties on different timescales. Experiments on MD simulations of HSA with explicit water molecules has been reported ⁶³. Based on the agreement of experimental and computational evidence, the best docking conformation of HSA-lupeol and HSA-lupeol derivative was chosen (Fig. 7A and 7D) and used as the starting point for a 10 ns simulation. After a series of 10 ns MD simulations, the trajectories were analyzed for stability and the complete details of motions of protein and ligands in the system. Properties like root mean square deviation (RMSD), radius of gyration (R_g) and root mean square fluctuations (RMSF) of HSA-ligand complexes were examined, with respect to the unliganded HSA, which could explain the experimentally observed activity and to cross check our results from docking.

An initial evaluation of structural drift is provided by analysis of the $C\alpha$ atom RMSDs from the initial structures as a function of time. The RMSD values of $C\alpha$ atoms in unliganded HSA and HSA-lupeol and HSA-lupeol derivative complexes were shown in Fig. 8A and 8B. From 0-10 ns trajectory data, the rmsd values for free HSA is 0.4 ± 0.3 nm, while the HSA-lupeol complex fluctuated initially, and got stabilized after 3 ns simulation time with the data points 0.3 ± 0.5 nm (Fig. 8A). HSA-lupeol derivative showed less fluctuation of heavy atoms compared to HSA-lupeol complex, and all the heavy atoms are around 0.35 ± 0.2 to 0.38 ± 0.2 , respectively (Fig. 8B). This indicated that, with only few atomic fluctuations in the magnitude of RMSD of both systems, protein-ligand complex reached to an equilibrium state. The interval conformations during MD simulation was observed to check whether the ligand was anchored to the residues in the active site using VMD software⁶⁴, which confirmed that the ligand anchored into the active site during the 10 ns MD simulation (data not shown). Hence, we conclude that during simulations the complexes remain stable and no significant structural drift occurred from the initial docked conformers.

The variation of R_g with time is depicted in Fig. 8C and 8D, which explains the compactness of the system (protein + ligand), over the course of MD simulations. The R_g values of unliganded HSA is at 2.65 ± 0.35 nm, while the complexes initially fluctuated and then achieved equilibrium after 5 ns at around 2.6 ± 0.003 and 2.58 ± 0.023 nm for lupeol and lupeol derivative, indicating the stabilization of the complex. The earlier report shows that the R_g value of HSA was experimentally measured in aqueous solution and reported to be 2.74 ± 0.035 ⁶⁵. However, there is a decrease in R_g value, upon binding of lupeol and lupeol derivative, which can corroborate with the similar results obtained from free HSA 2.59 ± 0.03 and upon HSA- β -sitosterol complex 2.40 ± 0.031 nm, betulinic acid stabilized from 2.59 ± 0.03 to 2.51 ± 0.01 nm

and it can also be observed from R_g of chitosan oligomers stabilizing at 2.52 ± 0.03 to 2.45 ± 0.031 ^{18,20,40}, while some ligands like fatty acids (myristates) showed increase in R_g value upon binding with HSA⁶⁶. This indicates that these compounds changes the microenvironment of HSA while binding and further leads to the conformational changes. The above observations also supports the changes observed in CD data, as discussed above (Fig. 6C). Thus the RMSD and R_g results suggest that HSA flexibility enable preferential affinity for several ligands.

Investigation of local protein mobility of HSA-lupeol and HSA-lupeol derivative complexes explains the root mean square fluctuation of all residues over a 10 ns time scale. The RMSF values of HSA-lupeol and HSA-lupeol derivative overlap with the RMSF values of unliganded HSA and these are plotted against residue numbers. Our results showed less atomic fluctuations at ligand binding sites I and II, with respect to other domain regions as shown in Fig. 9A and 9B. To investigate in details of atomic fluctuations at drug-binding sites, the RMSF value of each amino acid residue at the site was determined. Fig. 9C and 9D focus on the residues Pro416, Ser419, Thr467, Pro468, Val469, Ser470, Asp471, Thr498, Tyr497, Val498, surrounding the binding pocket of lupeol in the region of site II, and residues Ala300, Asp301, Leu302, Pro303, Ser304, Met298, Arg337, His338, Val381, Phe374, Lys378, Gln442, Met446, Pro299, surrounding lupeol derivative in site I. In the present MD study, many of the residues showed smaller RMSF values, suggesting that amino acids that can affect binding affinity in HSA molecules have smaller atomic fluctuations; in other words, these amino acid residues are rigid as compared with other residues. The structural movements of HSA domain display different binding site properties which can help the ligands to adopt different binding modes, as observed in the docking result (Fig. 7B and 7E). Consequently, different free energy values are obtained from fluorescence binding studies and computational results (Table S3).

MD simulations confirmed that there is significant movement of the protein after binding of ligand molecules, which can influence on ligand recognition ⁶⁷. To analyze the internal motions of HSA-lupeol complexes, snapshots were taken at each nanosecond interval, to understand the flexibility of ligand in interacting with the residues of HSA in binding pocket during the simulation. Fig. S4 shows the snapshot taken at 0.1 ns, where the lupeol molecule is formed hydrogen bond with Asn471, as we can also see in the docking conformer. While at 3 ns, residing in the subdomain IIIA, there is a slight relative motions of lupeol showing hydrogen bond with Val498, which is a part of intradomain connection between IIIA and IIIB ⁹⁹, and stabilized until 10 ns. These movements were supported by RMSD C α deviation and radius of gyration, discussed earlier (Fig. 8A and 8C). Although lupeol derivative did not show hydrogen bonding with any of the protein residues, the 10ns MD simulation indicates that it is stable around the binding site, compared with lupeol binding to HSA (Fig. S5). Due to these structural arrangements, there is a change in microenvironment observed during fluorescence emission shown in Fig. 3B, and also secondary conformational changes of HSA, discussed through CD studies (Fig. 6B). This proves that the lupeol derivative is stable in the hydrophobic cavity of HSA, changing its orientation while binding to HSA as showed in the above docking studies. Thus, we suggest that the changes in atomic fluctuations observed in the present MD study influence the binding affinity of both these drugs.

Conclusions

The goal of this study was to elucidate the effect of binding of phytochemicals i.e., lupeol and lupeol derivative to HSA and AGP. Lupeol and its derivative were checked for their potency in binding with the plasma proteins. Also, these molecules showed a decrease in viability of inflammatory macrophages and human cervical cancer cells. IL-1 β and IL-6 cytokines

expression was down regulated by lupeol and lupeol derivative indicating strong inhibition of inflammatory cells. Percent apoptotic cells are raised with lupeol derivative than lupeol indicate both molecules have anti-cancer activity. Slight difference in cytotoxic studies may be due to a single double bond position difference in both molecules, addition of functional groups may induce more changes in their activity. Lupeol and lupeol derivative bind to HSA and AGP, change in fluorescence quenching reveals a change in microenvironment around the binding pocket. Site-specific binding studies indicate that lupeol binds in site II whereas lupeol derivative binds to site I, replacing ibuprofen and phenyl butazone, respectively. Further CD studies revealed partial unfolding of the protein upon binding of lupeol, however, the degree of unfolding is significantly greater when binding lupeol derivative. Additionally, the molecular docking studies corroborated with the experimental study indicating that lupeol binds to subdomain IIIA of site II and lupeol derivative to subdomain IIA of site I, with hydrophobic and hydrogen bonding interactions. The primary HSA drug binding sites II and I, showed relatively small RMSF values on average, underscoring the stability of HSA-lupeol and HSA-lupeol derivatives after complex formation. Simulations over longer time periods are preferable for further detailed investigation of the effect of binding. The present study, successfully provided insights of lupeol and lupeol derivative and their surrounding residues of HSA, over a period of time. The structural rearrangements and partial changes are in agreement with CD studies, RMSD and Rg values. Our study provides useful and accurate information about HSA/AGP-lupeol, HSA/AGP-lupeol derivative interactions. Thus, these studies will certainly give an understanding of synthesizing new inspired lupeol drug to act upon life threatening diseases.

Acknowledgements

This work was supported by Department of Science and Technology (No. SR/SO/BB-0123/2010 and DST-FIST), DBT-CREBB, India and UPE-2, University of Hyderabad. We thank CIL and BIF, University of Hyderabad, for CD and Bioinformatics facilities. The author Dr. K. Monika is grateful to UGC-NEW Delhi for providing financial support under the scheme of Dr. D. S. Kothari Postdoctoral Fellowship.

References

1. K. Papi Reddy, A. Singh, A. Puri, A. Srivastava and T. Narender, *Bioorganic & medicinal chemistry letters*, 2009, **19**, 4463-4466.
2. S. V, K. SA, S. PT and V. P, *Vascul Pharmacol*, 2007, **46**, 412-418.
3. H. R. Siddique, S. K. Mishra, R. J. Karnes and M. Saleem, *Clinical Cancer Research*, 2011, **17**, 5379-5391.
4. G. Kweifio - Okai, B. Field, B. A. Rumble, T. A. Macrides and F. De Munk, *Drug development research*, 1995, **35**, 137-141.
5. M. A. Fernández, B. Heras, M. D. Garcia, M. T. Sáenz and A. Villar, *Journal of Pharmacy and Pharmacology*, 2001, **53**, 1533-1539.
6. M. Shahlai, S. M. Ghanadian, A. M. Ayatollahi, M. A. Mesaik, O. M. Abdalla, S. Afsharypour and M. Rabbani, *Medicinal Chemistry Research*, 2013, **22**, 1795-1803.
7. P. Ascenzi and M. Fasano, *Biophysical chemistry*, 2010, **148**, 16-22.
8. X. M. He and D. C. Carter, 1992.
9. U. Kragh-Hansen, *Pharmacological Reviews*, 1981, **33**, 17-53.
10. T. Peters Jr, *Advances in protein chemistry*, 1985, **37**, 161-245.
11. U. Kragh-Hansen, V. T. G. Chuang and M. Otagiri, *Biological and Pharmaceutical Bulletin*, 2002, **25**, 695-704.
12. M. Fasano, S. Curry, E. Terreno, M. Galliano, G. Fanali, P. Narciso, S. Notari and P. Ascenzi, *IUBMB life*, 2005, **57**, 787-796.
13. C.-E. Ha and N. V. Bhagavan, *Biochimica et Biophysica Acta (BBA)-General Subjects*, 2013, **1830**, 5486-5493.
14. G. Sudlow, D. Birkett and D. Wade, *Molecular Pharmacology*, 1976, **12**, 1052-1061.
15. A. Varshney, P. Sen, E. Ahmad, M. Rehan, N. Subbarao and R. H. Khan, *Chirality*, 2010, **22**, 77-87.
16. S. Curry, *Drug metabolism and pharmacokinetics*, 2009, **24**, 342-357.
17. B. Sudhamalla, M. Gokara, N. Ahalawat, D. G. Amooru and R. Subramanyam, *The Journal of Physical Chemistry B*, 2010, **114**, 9054-9062.
18. S. Neelam, M. Gokara, B. Sudhamalla, D. G. Amooru and R. Subramanyam, *The Journal of Physical Chemistry B*, 2010, **114**, 3005-3012.
19. M. Gokara, T. Malavath, S. K. Kalangi, P. Reddana and R. Subramanyam, *Journal of Biomolecular Structure and Dynamics*, 2014, **32**, 1290-1302.
20. A. Garg, D. M. Manidhar, M. Gokara, C. Mallela, C. S. Reddy and R. Subramanyam, *PloS one*, 2013, **8**, e63805.
21. S. Afrin, G. Rabbani and R. H. Khan, *Journal of Luminescence*, 2014, **151**, 219-223.
22. M. Gokara, B. Sudhamalla, D. G. Amooru and R. Subramanyam, *PloS one*, 2010, **5**, e8834.
23. W. Zhang, X. Bai, Y. Wang, B. Zhao, Y. Zhao, W. Hou, Y. Jin and D. Zhao, *Spectrochimica Acta Part A: Molecular and Biomolecular Spectroscopy*, 2014, **117**, 210-215.
24. D. P. Yeggoni, M. Gokara, D. Mark Manidhar, A. Rachamalla, S. Nakka, C. S. Reddy and R. Subramanyam, *Molecular pharmaceutics*, 2014, **11**, 1117-1131.
25. I. Petitpas, T. Grüne, A. A. Bhattacharya and S. Curry, *Journal of molecular biology*, 2001, **314**, 955-960.
26. F. Zsila, *Molecular pharmaceutics*, 2013, **10**, 1668-1682.

27. R. Subramanyam, M. Goud, B. Sudhamalla, E. Reddeem, A. Gollapudi, S. Nellaepalli, V. Yadavalli, M. Chinnaboina and D. G. Amooru, *Journal of Photochemistry and Photobiology B: Biology*, 2009, **95**, 81-88.
28. T. Fournier, N. Medjoubi-N and D. Porquet, *Biochimica et Biophysica Acta (BBA)-Protein Structure and Molecular Enzymology*, 2000, **1482**, 157-171.
29. V. Kopecký, R. Ettrich, K. Hofbauerová and V. Baumruk, *Journal of Spectroscopy*, 2004, **18**, 323-330.
30. V. T. G. Chuang and M. Otagiri, *Chirality*, 2006, **18**, 159-166.
31. J. R. Simard, P. A. Zunszain, J. A. Hamilton and S. Curry, *Journal of molecular biology*, 2006, **361**, 336-351.
32. C. Gambacorti-Passerini, M. Zucchetti, D. Russo, R. Frapolli, M. Verga, S. Bungaro, L. Tornaghi, F. Rossi, P. Pioltelli and E. Pogliani, *Clinical Cancer Research*, 2003, **9**, 625-632.
33. R. Subramanyam, A. Gollapudi, P. Bonigala, M. Chinnaboina and D. G. Amooru, *Journal of Photochemistry and Photobiology B: Biology*, 2009, **94**, 8-12.
34. T. Mosmann, *Journal of immunological methods*, 1983, **65**, 55-63.
35. G. Zhang, V. Gurtu, S. R. Kain and G. Yan, *Biotechniques*, 1997, **23**, 525-531.
36. J. R. Lakowicz and I. Gryczynski, *Biophysical chemistry*, 1992, **45**, 1-6.
37. M. Mansouri, M. Pirouzi, M. R. Saberi, M. Ghaderabad and J. Chamani, *Molecules*, 2013, **18**, 789-813.
38. G. M. Morris, D. S. Goodsell, R. Huey and A. J. Olson, *Journal of computer-aided molecular design*, 1996, **10**, 293-304.
39. G. M. Morris, R. Huey, W. Lindstrom, M. F. Sanner, R. K. Belew, D. S. Goodsell and A. J. Olson, *Journal of computational chemistry*, 2009, **30**, 2785-2791.
40. C. Malleada, N. Ahalawat, M. Gokara and R. Subramanyam, *Journal of molecular modeling*, 2012, **18**, 2589-2597.
41. A. C. Wallace, R. A. Laskowski and J. M. Thornton, *Protein engineering*, 1995, **8**, 127-134.
42. T. C. Guizado, *Journal of molecular modeling*, 2014, **20**, 1-13.
43. W. F. van Gunsteren, X. Daura and A. E. Mark, *Encyclopedia of computational chemistry*, 1998.
44. A. W. Schuttelkopf and D. M. Van Aalten, *Acta Crystallographica Section D: Biological Crystallography*, 2004, **60**, 1355-1363.
45. J. Hermans, H. J. Berendsen, W. F. Van Gunsteren and J. P. Postma, *Biopolymers*, 1984, **23**, 1513-1518.
46. C. Adcock, G. R. Smith and M. S. Sansom, *Biophysical journal*, 1998, **75**, 1211-1222.
47. H. J. Berendsen, J. P. M. Postma, W. F. van Gunsteren, A. DiNola and J. Haak, *The Journal of chemical physics*, 1984, **81**, 3684-3690.
48. T. Darden, D. York and L. Pedersen, *The Journal of chemical physics*, 1993, **98**, 10089-10092.
49. B. Hess, H. Bekker, H. J. Berendsen and J. G. Fraaije, *Journal of computational chemistry*, 1997, **18**, 1463-1472.
50. M. Saleem, *Cancer letters*, 2009, **285**, 109-115.
51. J. Vasconcelos, M. Teixeira, J. Barbosa-Filho, A. Lúcio, J. Almeida, L. de Queiroz, R. Ribeiro-dos-Santos and M. Soares, *International immunopharmacology*, 2008, **8**, 1216-1221.
52. J. Ghuman, P. A. Zunszain, I. Petitpas, A. A. Bhattacharya, M. Otagiri and S. Curry, *Journal of molecular biology*, 2005, **353**, 38-52.
53. A. Sułkowska, *Journal of Molecular Structure*, 2002, **614**, 227-232.
54. N. Tayeh, T. Rungassamy and J. R. Albani, *Journal of pharmaceutical and biomedical analysis*, 2009, **50**, 107-116.
55. D. Agudelo, P. Bourassa, J. Bruneau, G. Bérubé, É. Asselin and H.-A. Tajmir-Riahi, *PloS one*, 2012, **7**, e43814.
56. L. Liang, H. Tajmir-Riahi and M. Subirade, *Biomacromolecules*, 2007, **9**, 50-56.
57. C. Dufour and O. Dangles, *Biochimica et Biophysica Acta (BBA)-General Subjects*, 2005, **1721**, 164-173.
58. M. Gokara, G. B. Kimavath, A. R. Podile and R. Subramanyam, *Journal of Biomolecular Structure and Dynamics*, 2013, 1-15.
59. M. H. Rahman, K. Yamasaki, Y. Shin, C. C. Lin and M. Otagiri, *Biological & pharmaceutical bulletin*, 1993, **16**, 1169-1174.
60. Z. Sattar, H. Iranfar, A. Asoodeh, M. R. Saberi, M. Mazhari and J. Chamani, *Spectrochimica Acta Part A: Molecular and Biomolecular Spectroscopy*, 2012, **97**, 1089-1100.
61. T. Kosa, T. Maruyama and M. Otagiri, *Pharmaceutical research*, 1998, **15**, 449-454.
62. S. Sugio, A. Kashima, S. Mochizuki, M. Noda and K. Kobayashi, *Protein engineering*, 1999, **12**, 439-446.
63. R. Artali, G. Bombieri, L. Calabi and A. Del Pra, *Il Farmaco*, 2005, **60**, 485-495.
64. W. Humphrey, A. Dalke and K. Schulten, *Journal of molecular graphics*, 1996, **14**, 33-38.

65. M. Kiselev, I. Gryzunov, G. Dobretsov and M. Komarova, *Biofizika*, 2000, **46**, 423-427.
66. S. i. Fujiwara and T. Amisaki, *Proteins: Structure, Function, and Bioinformatics*, 2006, **64**, 730-739.
67. H. A. Carlson, K. M. Masukawa and J. A. McCammon, *The Journal of Physical Chemistry A*, 1999, **103**, 10213-10219.

Figure Legends

Fig. 1 Cytotoxicity of lupeol and lupeol derivative. (A) lupeol and (B) lupeol derivative (Ld) showing anti-inflammatory property against LPS induced mouse macrophages (RAW 264.7) in a dose dependent manner. (C) lupeol and (D) lupeol derivative showing anti-cancer property against human cervical cancer cells (HeLa). Cell growth was measured by the MTT assay and the IC₅₀ values are calculated for their inhibition.

Fig. 2 Apoptosis induction of 15 μ M lupeol and 12 μ M lupeol derivative on 24h culture of HeLa cell line. The fluorescence was determined immediately by using flow cytometer. Cells were estimated as percentages in quadrants, i.e. Q1 as late apoptotic or necrotic cells, Q2 dead cells, Q3 as live cells and Q4 as apoptotic cells.

Fig. 3 Fluorescence emission spectra of HSA-ligands, $\lambda_{ex} = 285$ nm, temperature 25° C. (A) free HSA (0.001 mM) and different concentrations of lupeol (0.001 – 0.009 mM). (B) free HSA and different concentrations of lupeol derivative (Ld). Plots of log (dF/F) against log [Q]. $\lambda_{ex} = 285$ nm, $\lambda_{em} = 362$ nm.

Fig. 4 Fluorescence emission spectra of AGP-ligands, $\lambda_{ex} = 285$ nm, temperature 25° C. (A) free AGP (0.001 mM) and different concentrations of lupeol (0.001 – 0.009 mM). (B) free AGP and different concentrations of lupeol derivative (Ld). Plots of log (dF/F) against log [Q] $\lambda_{ex} = 285$ nm, $\lambda_{em} = 340$ nm.

Fig. 5 Site-specific binding of ligands with HSA. (A) displacement of ibuprofen from the HSA-ibuprofen complex by lupeol. (B) displacement of phenyl butazone from the HSA-phenyl

butazone by lupeol derivative (Ld).

Fig. 6 CD spectra of free HSA and HSA+lupeol, lupeol derivative complexes. (A) HSA and HSA -lupeol complex. (B) HSA and HSA -lupeol derivative complex with a protein concentration of 0.001 mM and ligand concentrations of 0.001, 0.002 and 0.003 mM. (C) Percentage concentrations of lupeol and lupeol derivative (Ld).

Fig. 7 Best docking conformation with lowest binding energy. (A) Lupeol bound to IIIA domain on HSA and (D) lupeol derivative to IIA (Protein and ligand colored in magenta and red, respectively) (B) Stereoview of docking pose of HSA-lupeol complex and (E) HSA-lupeol derivative complex (prepared by using Pymol v 1.5) (C) Ligplot showing hydrophobic interactions of HSA-lupeol and (F) HSA-lupeol derivative in the binding sites.

Fig. 8 Time dependence of RMSD of $C\alpha$ atoms from the starting structure during 10 ns MD simulations. (A) Plot of rmsd values for unliganded HSA and HSA-lupeol (B) unliganded HSA and HSA-lupeol derivative (Ld) complex. (C) Time evolution of the radius of gyration (Rg) during 10 ns of MD simulation of unliganded HSA and HSA-lupeol (D) unliganded HSA and HSA-lupeol derivative complexes.

Fig. 9 Comparison of the RMSF of $C\alpha$ atoms along the sequence derived from the 10 ns simulations. (A) Red line represents the unliganded HSA and black line the HSA-lupeol complex. (B) HSA-lupeol derivative complex. (C) The RMSF values of free HSA and HSA-lupeol (D) HSA-lupeol derivative (Ld) complexes were plotted against residue numbers. Residues showing rigidity in the subdomain IIIA and IIA.

Figure 1

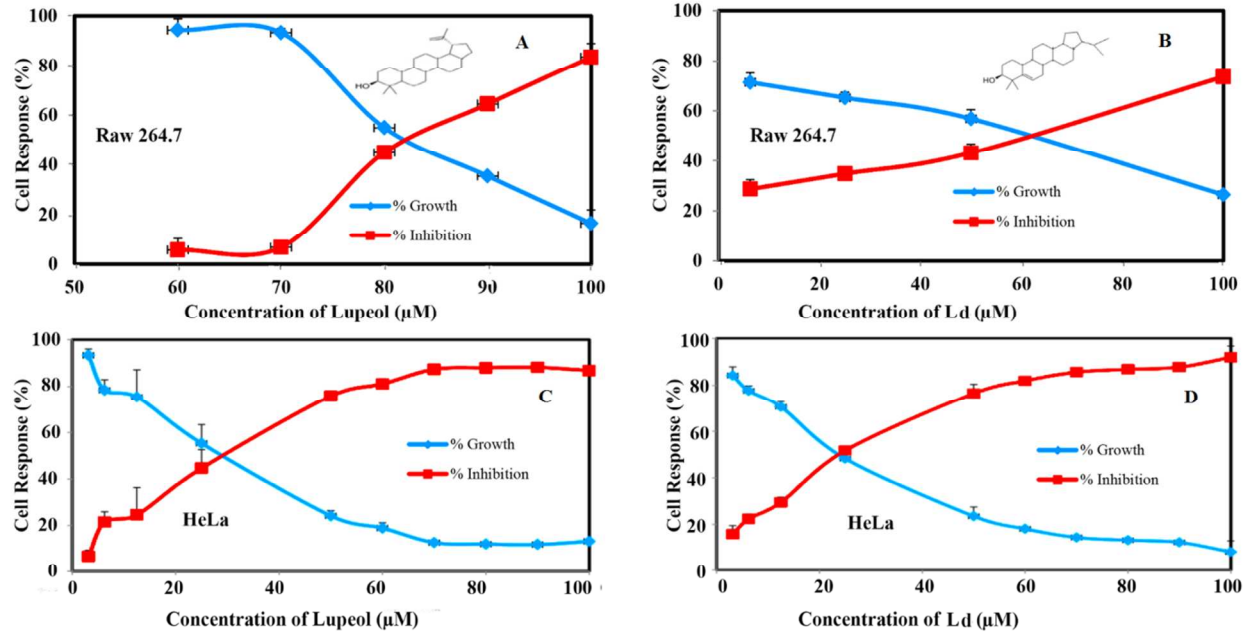


Figure 2

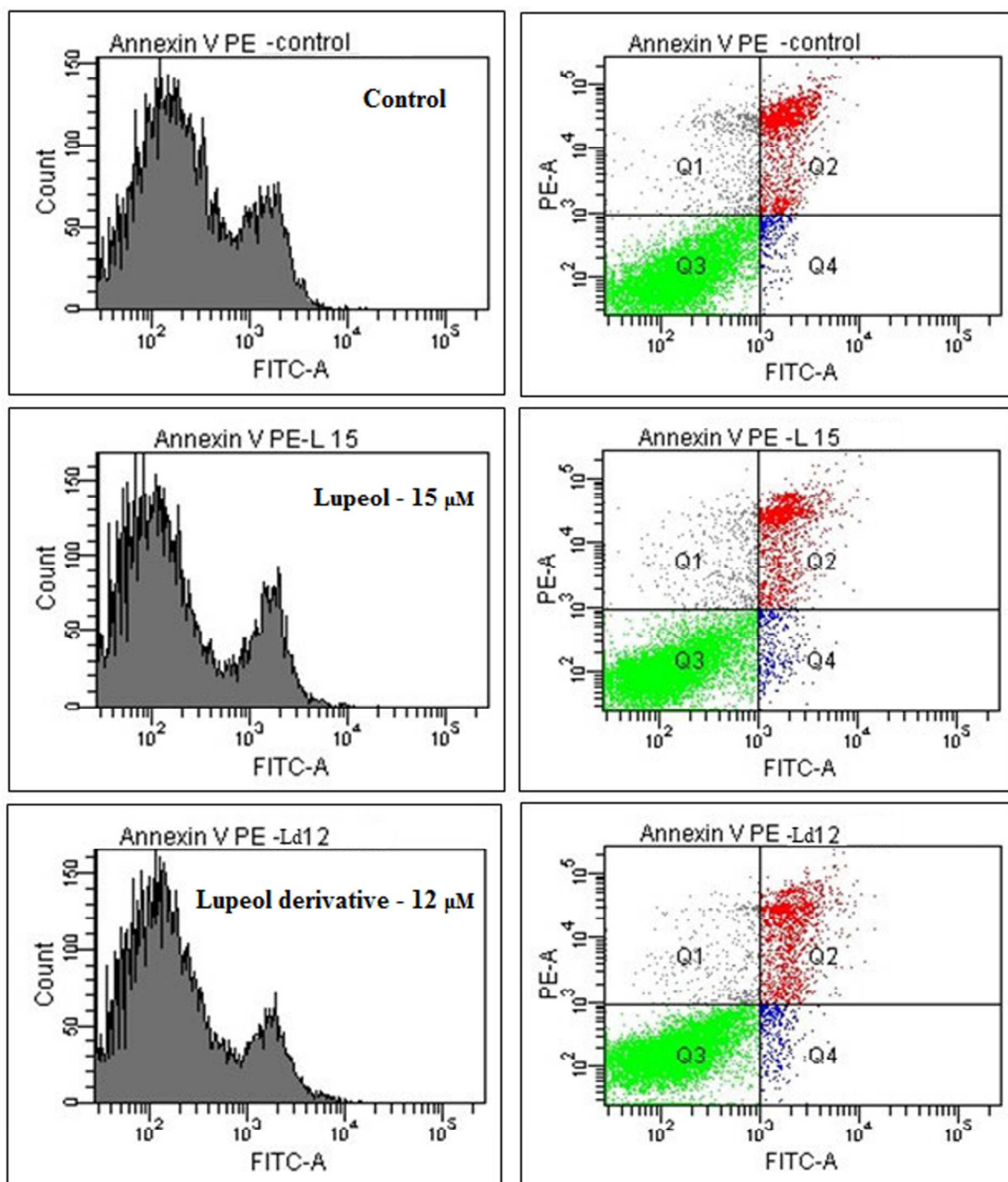


Figure 3

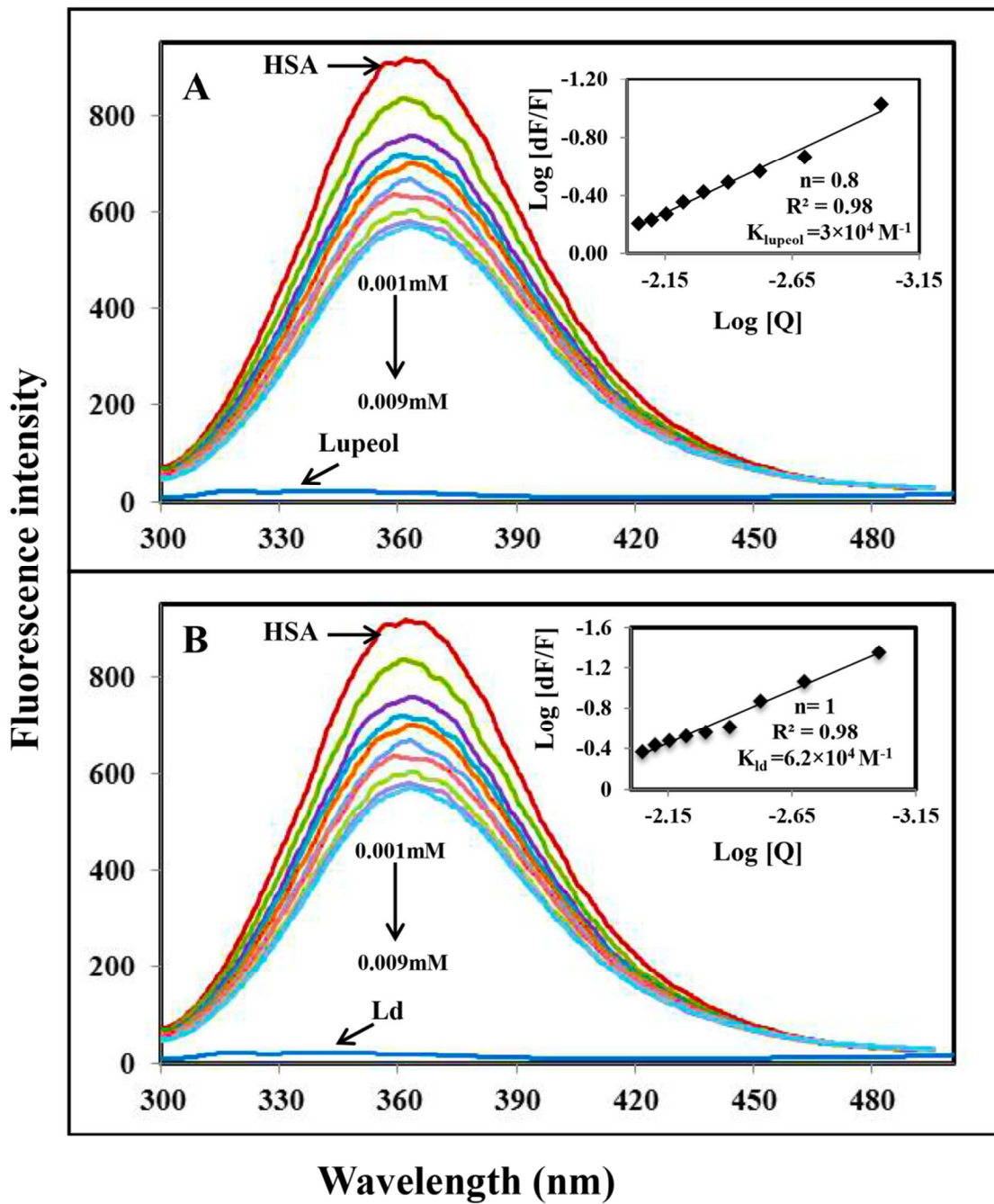


Figure 4

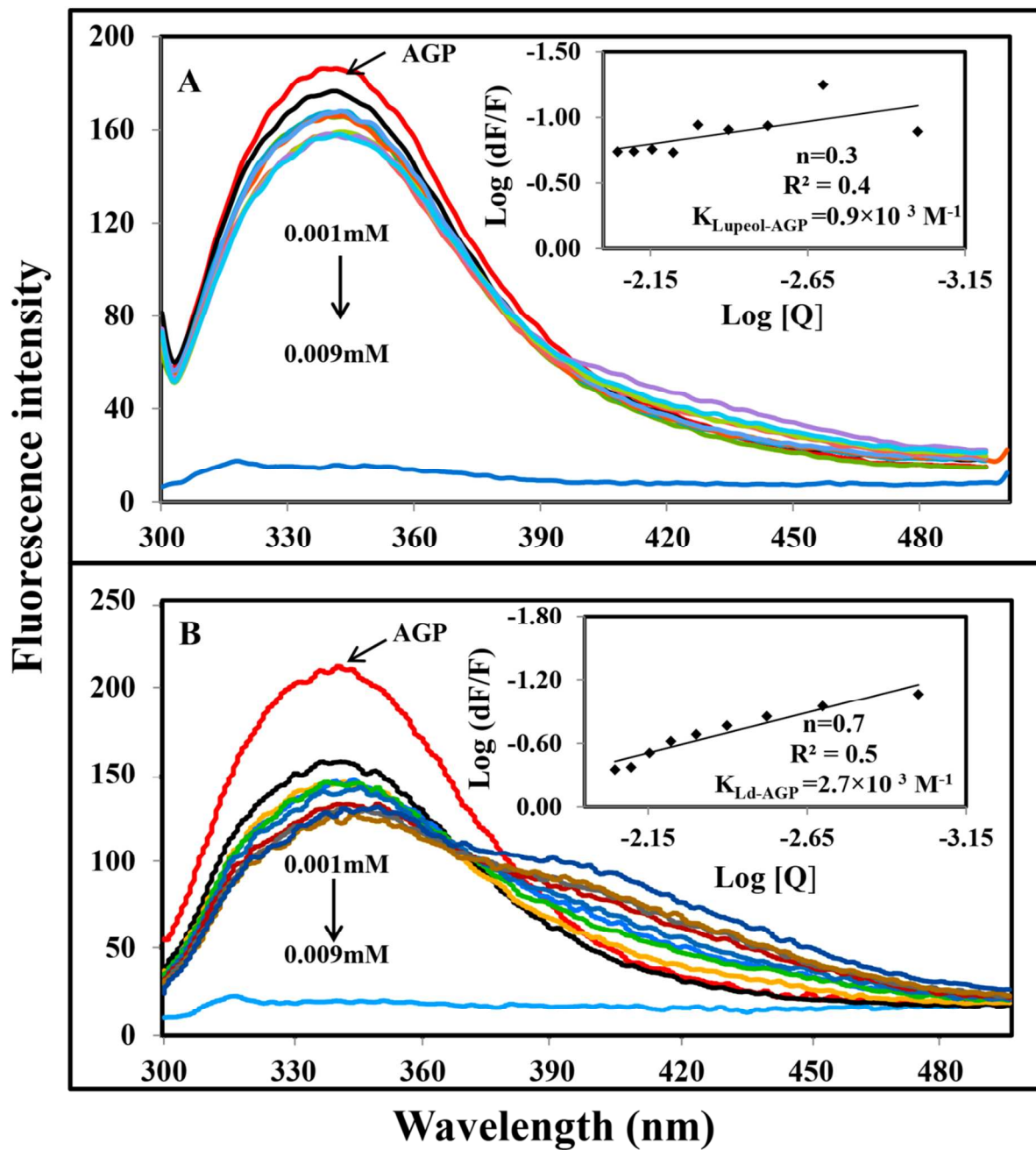


Figure 5

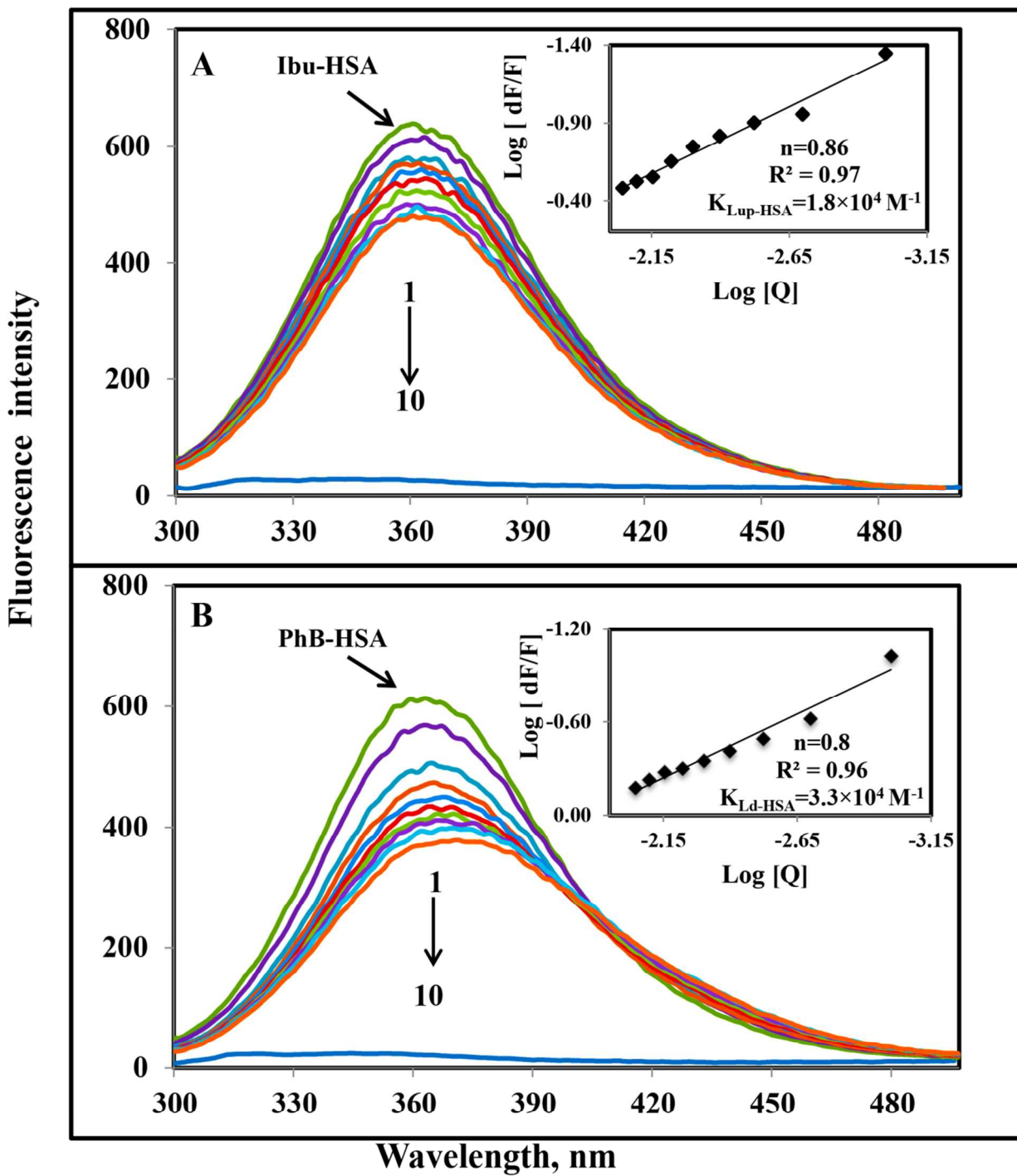


Figure 6

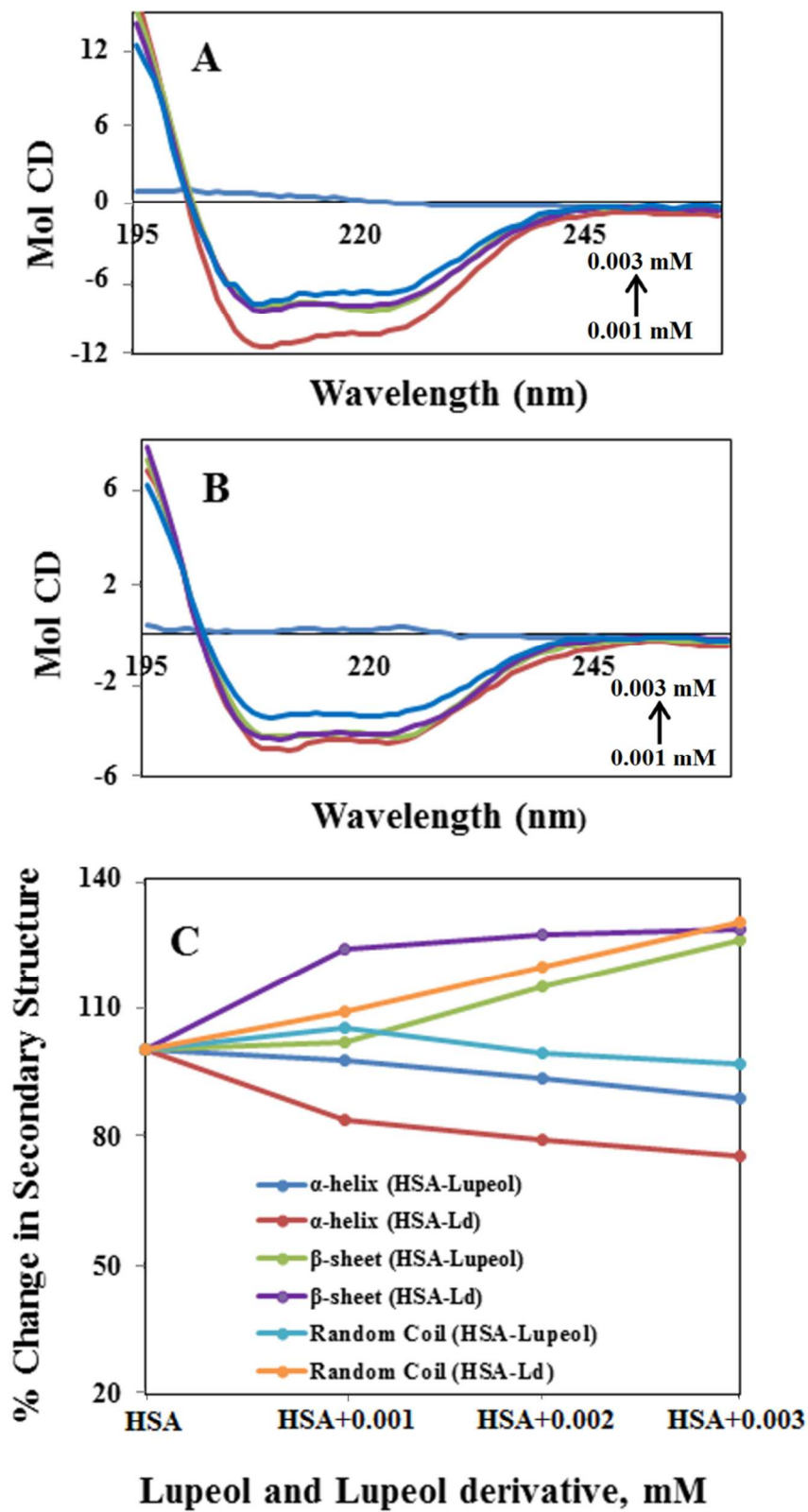


Figure 7

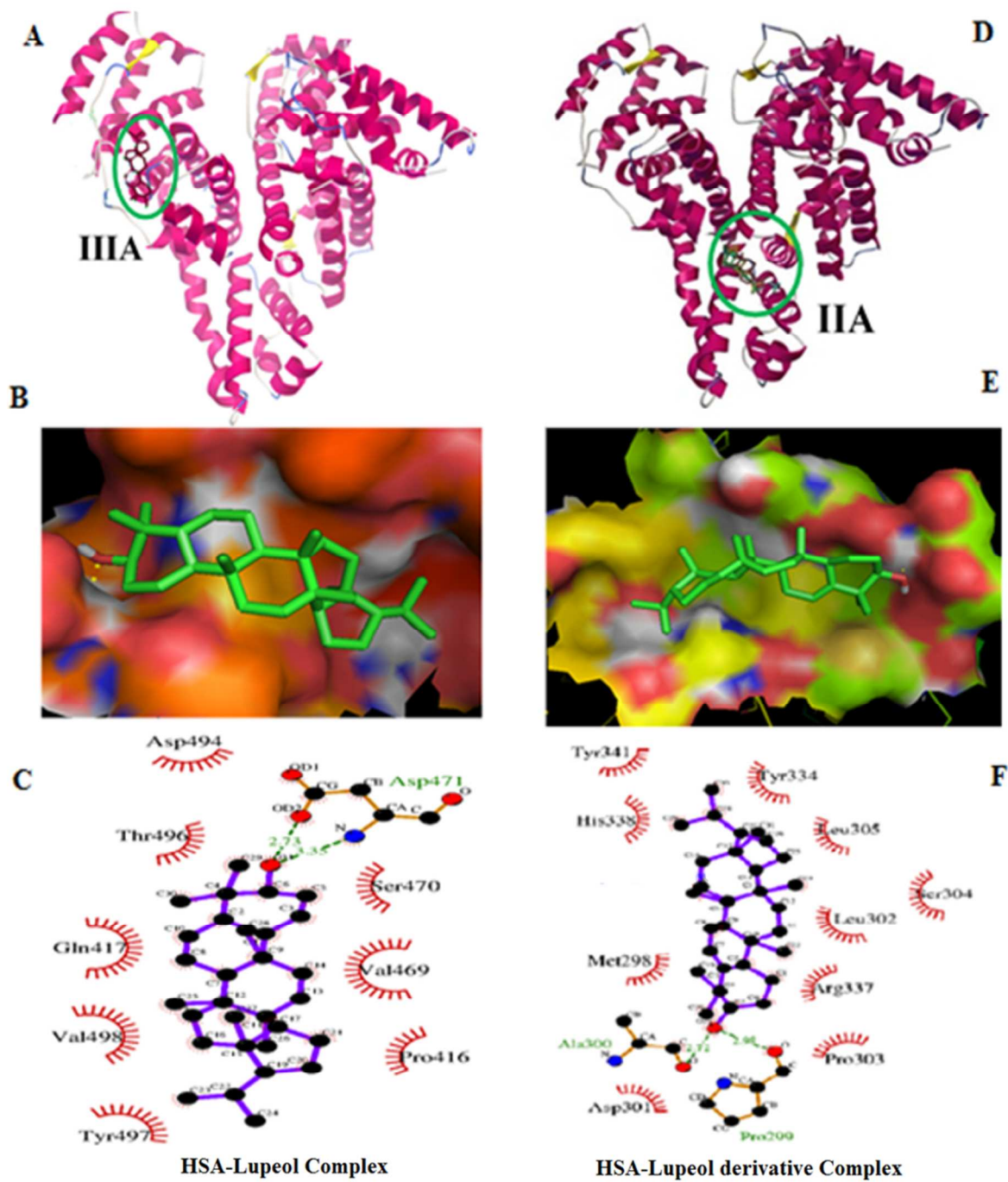


Figure 8

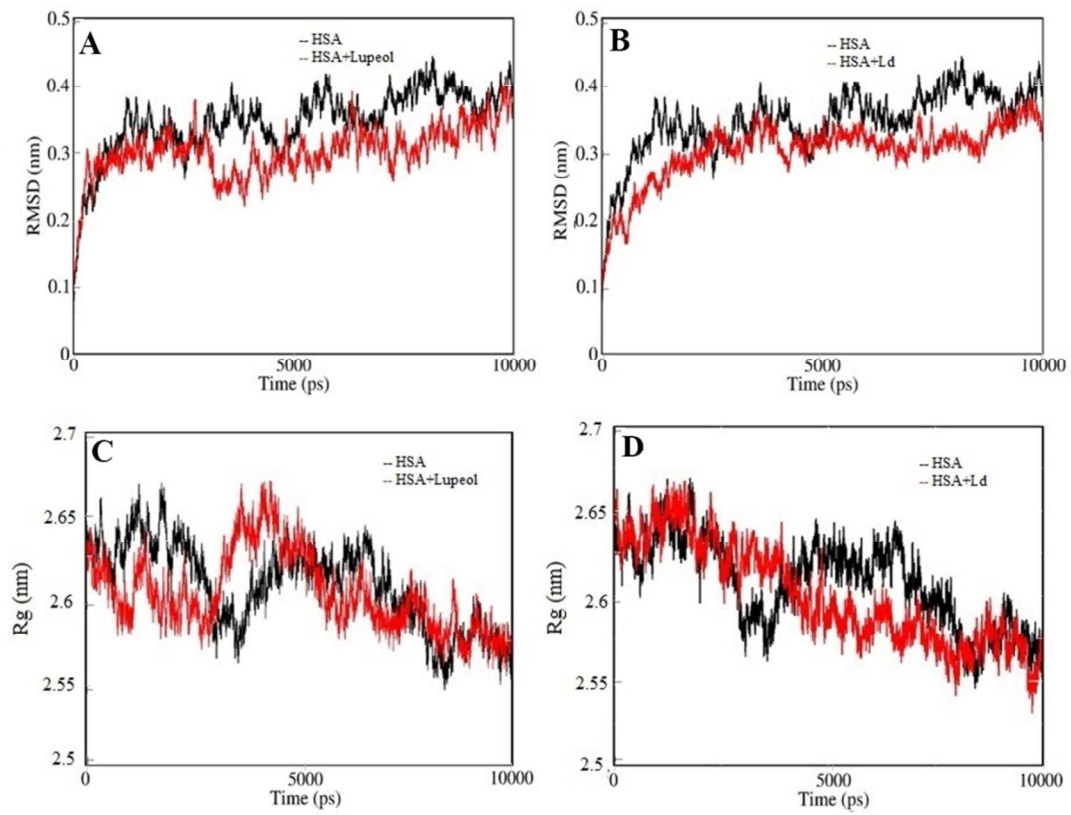


Figure 9

